

Designing rare-earth free permanent magnets in Heusler alloys via interstitial doping

Qiang Gao^a, Ingo Opahle^a, Oliver Gutfleisch^{a,b}, Hongbin Zhang^a

^a*Institut für Materialwissenschaft, Technische Universität Darmstadt, 64287, Darmstadt, Germany*

^b*Fraunhofer-Research Institution Materials Recycling and Resource Strategies IWKS, 63457, Hanau, Germany*

Abstract

Based on high-throughput density functional theory calculations, we investigated the effects of light interstitial H, B, C, and N atoms on the magnetic properties of cubic Heusler alloys, with the aim to design new rare-earth free permanent magnets. It is observed that the interstitial atoms induce significant tetragonal distortions, leading to 32 candidates with large (> 0.4 MJ/m³) uniaxial magneto-crystalline anisotropy energies (MAEs) and 10 cases with large in-plane MAEs. Detailed analysis following the the perturbation theory and chemical bonding reveals the strong MAE originates from the local crystalline distortions and thus the changes of the chemical bonding around the interstitials. This provides a valuable way to tailor the MAEs to obtain competitive permanent magnets, filling the gap between high performance Sm-Co/Nd-Fe-B and widely used ferrite/AlNiCo materials.

Key words: Permanent magnets, Interstitial, Tetragonal distortion, Magneto-crystalline anisotropy energy

2010 MSC: 00-01, 99-00

*Corresponding author

Email addresses: hzhang@tmm.tu-darmstadt.de (Hongbin Zhang)

1. Introduction

Permanent magnets are of great technical importance for many key technologies such as electric vehicles, wind turbines, and automation and robotics to name only a few [1]. Looking at the intrinsic magnetic properties, such materials demand a large magneto-crystalline anisotropy energy (MAE), a sizable saturation magnetization, and a high Curie temperature. The MAE originates from the spin-orbit coupling (SOC) and sets an upper limit for the microstructure dependent coercivity of permanent magnets. At present, rare-earth magnets based on Sm-Co (MAE: 17.0 MJ/m³, Magnetization (M_s): 910 kA/m) and Nd-Fe-B (MAE: 5.0 MJ/m³, M_s : 720 kA/m) are prototypes of high performance permanent magnets, with a substantial cost and performance gap to other classes of commercially available permanent magnets such as AlNiCo (MAE: 0.04 MJ/m³, M_s : 50 kA/m) and ferrites (MAE: 0.03 MJ/m³, M_s : 125 kA/m) [2]. Thus, there is a great interest to develop novel permanent magnets so that the full spectra of applications can be achieved, ideally without critical elements such as rare-earth elements [3, 4].

An enlightening idea was proposed to achieve giant MAE in tetragonally distorted FeCo alloys [5], where both the tetragonal distortion and fine tuning of the number of electrons by alloying are crucial for the enhanced MAE. Follow-up experimental studies on FeCo alloys deposited on various substrates confirmed the theoretical prediction [6]. Nevertheless, due to the strong tendency for the FeCo alloys to relax, it is difficult to maintain the tetragonal distortion induced by the underlying substrates for thin films thicker than 2 nm [6, 7, 8]. Recently, following the prediction based on DFT calculations [9, 10], systematic studies have been performed on FeCo+X (X= C and B), where spontaneous tetragonal distortions with $c/a=1.04$ can be induced by a few atomic percent interstitial doping of C or B atoms occupying the octahedral interstitial sites. The resulting MAE can be as large as 0.5 MJ/m³ with B concentration up to 4 at%, where the tetragonal strain reaches 5%. For Fe_{0.38}Co_{0.62}, a large interstitial concentration of 9.6 at% B was achieved. [10] The effect of light interstitials on the magnetic

properties of body-centered cubic (BCC) iron has also been well studied. α -Fe with 12.5 at% content of nitrogen interstitial has been grown by sputtering on the MgO (100) substrates, leading to about 10% tetragonal distortion and significant enhancement of magnetization and MAE [11]. First-principle calculations and experimental results show that Fe with nitrogen interstitial has sizable MAE, favoring perpendicular magnetization [11]. Using the molecular beam epitaxy, boron has been incorporated into bcc Fe as interstitial dopants, which give rise to tetragonal distortions but the resulting MAE still favors in-plane magnetization due to tendency for B atoms to be agglomerated [12], where the interstitial content of B atoms can be as high as 14 at%.

Considering only the crystal structure, the austenite phase of Heusler alloys with the conventional cubic cell can be regarded as a $2 \times 2 \times 2$ supercell of the bcc lattice. In this regard, light interstitials such as H, B, C, and N can also be promising to induce significant tetragonal distortions and thus substantial MAE to Heusler alloys, like the FeCo alloys and bcc Fe. It is noted that the Heusler alloys in the tetragonal martensitic phase do show significant MAE. For instance, among 286 Heusler compounds, a systematic high throughput (HTP) screening suggests 19 potential tetragonal systems with large out-of-plane MAE (as large as 0.9 MJ/m^3) [13]. Matsushita *et al.* found 15 Heusler compounds have tetragonal distortions of which the MAEs ranges from -12 MJ/m^3 to 5.19 MJ/m^3 [14]. Focus on Ni based full Heusler compounds, Herper *et al.* [15] found tetragonal Ni_2FeGe has an MAE of 0.95 MJ/m^3 , which can be further increased to 1 to 2 MJ/m^3 by non-magnetic doping. Furthermore, imposing strain by proper substrates is helpful to engineer a large MAE out of the cubic Heusler alloys. It is found that the out-of-plane MAE of epitaxial Co_2MnGa (001) films can be remarkably enhanced from 0.11 MJ/m^3 to 0.33 MJ/m^3 by changing the substrate from ErAs/InGaAs/InP to ScErAs/GaAs [16]. Lastly, previous experiments have already demonstrated that interstitials can be incorporated into Heusler alloys, leading to enhanced mechanical stability and magnetocaloric effect [17, 18]. For $\text{Ni}_{43}\text{Mn}_{46}\text{Sn}_{11}\text{C}_x$, when the interstitial content x is increased from 0 to 8 the martensitic phase transformation temperature is increased from

196 to 249 K, while a remarkable increase of MAE is observed when x is increased from 0 to 2 [17]. Due to large loss of manganese in content of $x=8$, there is even a distortion of crystal structure from Hg_2CuTi -type to the Cu_2MnAl -type [17]. Similar effect has also been observed in $\text{Ni}_{50}\text{Mn}_{34.8}\text{In}_{14.2}$, $\text{Ni}_{43}\text{Mn}_{46}\text{Sn}_{11}$ and $\text{Ni}_{50}\text{Mn}_{38}\text{Sb}_{12}$ doped with B interstitial [18, 19, 20].

In this work, focusing on developing rare-earth free permanent magnets, we have performed high-throughput first-principles calculations to investigate the effects of light interstitials (*e.g.*, H, B, C, and N) on cubic Heusler alloys. After identifying the most favorable site preference of the interstitial atoms, the MAE of compounds with negative formation energy was evaluated to select the most promising candidates. Apart from thermodynamically stable criteria, the disorder effect should also be considered, which is however beyond the scope of the present paper and saved for future study. We observed that the induced MAE can be as large as 2.4 MJ/m^3 , and there are 32 systems with a sizable out-of-plane MAE ($\geq 0.4 \text{ MJ/m}^3$). Detailed analysis based on the Bain path and the atom-resolved MAE reveal that not only the global tetragonal distortion but also the associated local chemical bonding are crucial for the interstitial induced magnetic anisotropy.

2. Computational details

Starting with 128 full Heusler alloys with space group $\text{Fm}\bar{3}\text{m}$ including at least one of magnetic atoms Cr, Mn, Fe, Co, and Ni from the Inorganic Crystal Structure Database (ICSD) [21] (*cf.* Table A.1 in Appendix A), we performed density functional theory (DFT) calculations firstly to identify the energetically most favored interstitial sites for H, B, C, and N atoms. There are four types of interstitial sites based on the symmetries, as shown in Fig 1(a). The DFT calculations are managed with our in-house developed high-throughput environment (HTE) [22, 23], using both the Vienna ab initio Simulation Package (VASP) [24, 25] and full-potential local-orbital (FPLO) [26, 27] codes. The structure optimization is performed in a two step manner. Firstly, ultrasoft

pseudopotentials (US-PP) [28] are used in combination with the PW91 [29] exchange correlation functional, where the cutoff energy for the plane wave basis is set to 250 eV and a k -mesh density of 30\AA^{-1} . Secondly, the structure is relaxed using the projector augmented plane wave (PAW) method with the exchange-correlation functional under the generalized gradient approximation (GGA) parameterized by Perdew, Burke, and Ernzerhof (PBE) [30] with increasing plane wave expansion as 350 eV and k -mesh density as 40\AA^{-1} to achieve good convergence. After obtaining the energy lowest configuration, the MAEs of candidates with negative formation energy are calculated by using FPLO with a k -mesh density of 120\AA^{-1} to guarantee fine convergence. For the MAE calculations of Ni_2FeGa with C interstitial, the resulting k -mesh is set as $24 \times 24 \times 17$. The bonding analysis is done in terms of the crystal orbital Hamilton population (COHP) evaluated using the LOBSTER code [31].

3. Results and discussions

As shown in Fig. 1(a), the systems we considered correspond to doping 6.25 at% interstitial atoms (I) into the full Heusler alloys (X_2YZ), leading to a general chemical formula $\text{X}_2\text{YZI}_{1/4}$. This is in accordance with the typical doping concentrations experimentally accomplishable, *e.g.*, 12.5 at% content of N in Fe and 9.6 at% of B in $\text{Fe}_{0.38}\text{Co}_{0.62}$. [10, 11] Like Fe-Co alloys, we find light interstitials can indeed cause stable tetragonal distortion to cubic full Heusler alloys, which is quantized by the c/a ratio between the c -axis and in-plane lattice constants. As shown in Table 1, with N interstitials, Fe_2NiAl has the a tetragonal distortion as large as $c/a=1.57$. Such strong tetragonal distortions prevail in the other Heuslers with the other types of interstitial atoms, which break the cubic symmetry and hence lead to possible significant MAE. From the theoretical point of view, the MAE is defined as the total energy difference between the magnetization directions parallel to $[100]$ (in-plane) and $[001]$ (out-of-plane) directions as

$$\text{MAE} = E_{[100]} - E_{[001]} \quad (1)$$

where E_α is the total energy when magnetization direction is parallel to α . When the MAE value is positive (negative), the spontaneous magnetization will lie in the out-of-plane (in-plane) direction. Nevertheless, not all the interstitials are thermodynamically stable, as indicated by the formation energy. The candidates with an MAE more than 0.4 MJ/m^3 and a negative formation energy are listed in Table 1.

We notice all the parent Heusler compounds listed in Table 1 are ferromagnetic apart from Mn_2VGa and Rh_2NiSn . In our high throughput calculations, for convenience, all Heusler compounds are assumed to be ferromagnetic (FM). Previous studies [32, 33] have shown Rh_2MnAl is an antiferromagnet with Mn are antiferromagnetic coupling between nearest neighbors in the (111) plane, which is still in the same antiferromagnetic phase after incorporating C or N interstitials. As to Mn_2VGa , experimental research [34] has shown it is a half-metallic ferrimagnet with antiferromagnetic coupling between Mn and V with a total net saturation magnetization per formula unit as $1.88 \mu_B$ at 5 K. After inducing interstitial (C, B or N), Mn_2VGa is still ferrimagnetic with antiferromagnetic coupling between Mn and V, although initial spin configuration is ferromagnetic. Mn_2VGa have large MAE values as 1.82 MJ/m^3 , 1.50 MJ/m^3 and 1.26 MJ/m^3 with B, C and N interstitial, respectively. However, due to the ferrimagnetic phase, the resulting magnetization densities for Mn_2VGa with B, C and N interstitial are as weak as about $0.04\text{-}0.05 \mu_B/\text{\AA}^3$. Among all listed compounds in Table 1, Rh_2NiSn is weak ferromagnetic as experimental study [35] suggests it has a magnetic moment $0.6 \mu_B$ per formula unit. Our calculations demonstrate that H interstitials can induce a tetragonal distortion of $c/a=1.26$ and a sizable MAE value as 0.82 MJ/m^3 , whereas the magnetization is only about $0.02 \mu_B/\text{\AA}^3$.

As shown in Table 1, we found 32 compounds with a large out-of-plane MAE ($> 0.4 \text{ MJ/m}^3$) as well as 10 compounds with large in-plane MAE (absolute value larger than 0.4 MJ/m^3). In general, the interstitial atoms prefer to be located at the octahedral centers (including both the 24f and 24g sites) except for the H interstitials in Au_2MnAl which is stable at the tetrahedral center. For the

cases of octahedral center, the interstitials mostly prefers 24f sites $(\frac{1}{4}, 0, 0)$ where there are the same atoms in the plane perpendicular to the c-axis. On the other hand, for Co_2FeAl with N, Au_2MnAl with N and C, Ni_2MnSn with B, C and N, interstitials prefer 24g sites $(\frac{1}{2}, \frac{1}{4}, \frac{1}{4})$. We note that Fe_3Ge with H interstitial has the largest magnetization density as $0.13 \mu_{\text{B}} / \text{\AA}^3$ as well as quite large MAE value (1.50 MJ/m^3), indicating it is a promising permanent magnet. Furthermore, comparing with the magnetization and MAE of experimentally realized permanent magnets [1, 36, 37, 38, 39, 40] Heusler alloys with interstitials can fill the gap between the low performance magnets (such as AlNiCo and ferrite) and high performance magnets (such as Sm-Co and Nd-Fe-B) in terms of MAE and magnetization, which can spread a wide spectrum of applications.

Interestingly, Au_2MnAl with H is the only candidate where the interstitials prefer the tetrahedral center (16e site). However, for cases of Au_2MnAl with N and and C, interstitial prefers to be located in the octahedral centers with in-plane MAE. Such special interstitial behaviors can be easily understood based on the chemical bonding. Intuitively, due to the large atomic spheres of Au atoms, there is more space between the tetrahedron edge bound than the other Heusler compound. For instance, in Au_2MnAl with H, the bond length of H-Au pair in tetrahedral center (1.83 \AA) is comparable with that in octahedral center (1.93 \AA). On the other hand, the bond length of Cu-H pair for Cu_2MnAl with H in tetrahedral center is just 1.62 \AA , of which the value is obviously smaller than the H-Au pair for H interstitial in the tetrahedral center of Au_2MnAl (1.83 \AA). This suggests Au atom can really provide more space for interstitials in the tetrahedral site. It should be noticed that Cu-H pair in octahedral center also has a bit larger bond length (1.70 \AA) than that in tetrahedral center. However, in the tetrahedral center case, the bond length is too small to provide enough space for the interstitials. Thus, the H interstitials prefer the octahedral centers in Cu_2MnAl . On the other hand, for Au_2MnAl with C and N, it is observed that the interstitial atoms still prefer the octahedral center because of the larger atomic radii of C and N atoms compared to that of H. Therefore, in order to get the interstitials incorporated at the tetrahedral center, two conditions

should be satisfied: (a) The interstitial atoms should be small; (b) There should be large atoms in the parent compound, providing more space. Different site preference of the H and C/N interstitials induces significant changes on the MAE of Au_2MnAl , *e.g.*, H-interstitials favor out-of-plane magnetization while C/N interstitials lead to in-plane magnetization.

According to Table. 1, Fe_2CoGa with interstitials is a promising candidate for permanent magnets. However, in the ICSD database [21], Fe_2CoGa (ICSD ID: 102385 and 197615) and Fe_2CoGe (ICSD ID: 52954) are in the full Heusler structure, while early Mössbauer measurements have shown Fe_2CoGa and Fe_2CoGe are energetically favored in the inverse Heusler structure [41, 42]. Previous theoretical study [43] found that full Heusler Fe_2CoGa have a martensitic phase transition with a c/a ratio as 1.4, which is also confirmed by our calculation (*cf.* Fig. 2(a)). According to our Bain-path calculations, the inverse Heusler structure is still more energetically favored for Fe_2CoGa , even after considering H, B, C, and N interstitials. Nevertheless, after introducing interstitials, for the full Heusler structure, the c/a ratio is near to 1.4; whereas for the inverse Heusler structure, the c/a ratio of Fe_2CoGa with interstitials is just from 1.1-1.2 due to there is no metastable phase (Fig. 2(a)). The MAE values of the inverse Fe_2CoGa with B, C, N, and H interstitial are 0.1026 MJ/m^3 , 0.2148 MJ/m^3 , 0.3798 MJ/m^3 , and 0.1925 MJ/m^3 , respectively. Such lower MAE values are partially due to that interstitials induce much weaker tetragonal distortion to Fe_2CoGa for inverse Heusler structure ($1.1 \leq c/a \leq 1.2$) than that for full Heusler structure ($1.45 \leq c/a \leq 1.5$).

More interestingly, C, N, and H interstitials induce significant MAEs to Ni_2FeGa . Experimental studies suggest that Ni_2FeGa can be grown by melt-spinning technique [44] or glass-purify method [45], transforming from high chemical ordering $L2_1$ structure (full Heusler) to martensitic structure at 142 K with a high Curie temperature of 430 K[44]. Further experiments showed polycrystalline alloys $\text{Ni}_{53+x}\text{Fe}_{20-x}\text{Ga}_{27}$ have smaller but comparable entropy changes as classical magnetocaloric Heusler alloy systems Ni-Mn-Ga and Ni-Mn-Sn [46]. DFT calculations suggest that Ni_2FeGa has a tetragonal (corresponding

to the martensitic phase) structure of $c/a=1.35$ [47, 15] with an MAE as 0.318 MJ/m^3 [15]. We also found that Ni_2FeGa is stable in the tetragonal structure with a c/a ratio as 1.35 (Fig. 2(b)) and a comparable MAE as 0.2334 MJ/m^3 (0.0698 meV per chemical formula cell). However, the energy difference between tetragonal and cubic structures is as small as 2.80 meV/atom . As proposed by Barman, the martensite phase transition temperature is proportional to the energy difference between cubic and martensite phases [48], as manifested by the experimental martensitic transition at 142 K [44]. After inducing interstitial C, H, or N, Ni_2FeGa is stable in the tetragonal phase with $c/a \approx 1.40$. Correspondingly, the MAEs have been enhanced to 1.43 MJ/m^3 , 0.94 MJ/m^3 , and 0.56 MJ/m^3 for Heusler Ni_2FeGa with N, C, and H interstitials, respectively. Obviously, C and N interstitials cause more significant enhancement on the MAE than the H interstitials, though the resulting c/a ratios are comparable. Therefore, we suspect that both the tetragonal distortion and the chemical bonding environment will influence the MAE values for Heusler with interstitial, which will be discussed in detail below.

Turning now to the origin of the induced MAE by interstitials, from the theoretical perspective, beside the shape anisotropy due to the magnetic dipole-dipole interaction, the magneto-crystalline anisotropy (MCA) can be attributed to the spin-orbit coupling (SOC), which is the dominant contribution to MAE and hence coercivity for PMs. Based on the perturbation theory, Bruno [49] pointed out that the MCA can be formulated as

$$\text{MCA} = - \sum_i \frac{\xi_i}{4\mu_B} \Delta\mu_i, \quad (2)$$

where ξ_i denotes the atomic SOC constant and $\Delta\mu_i$ is the orbital moment difference between the magnetization directions parallel to $[001]$ and $[100]$ for the i -th atom. We note that such a model is best applicable for strong magnets where the majority spin channel is almost fully occupied, whereas there is a more general formula considering the spin-flip and quadruple terms [50]. Taking Ni_2FeGa as an example, Table 2 shows the atom-resolved orbital moments and the resulting contributions to the MCA using Bruno's formula, where the atomic

SOC constants for Ni and Fe are 630 cm^{-1} (corresponding to 78.1100 meV) and 400 cm^{-1} (corresponding to 49.5937 meV) taken from Ref. [51]. The resulting MCA for Ni_2FeGa with C, N, and H interstitials based on the Eq. (2) are 0.316 meV/f.u. , 0.528 meV/f.u. and 0.330 meV/f.u. , respectively. Correspondingly, the MAEs based on Eq. (1) are 0.296 meV/f.u. , 0.439 meV/f.u. and 0.167 meV/f.u. , respectively. The relative MAE differences of Bruno’s model to that of Eq. (1) are 17.17%, 23.83% and 79.61%. Nevertheless, the trend is correctly reproduced and we believe the atomic-resolved contributions evaluated based on Eq. 2 are still valuable to elucidate the origin of MCA. It is noteworthy that the tetragonal distortion ratios for Ni_2FeGa with H, C and N interstitial are 1.39, 1.40 and 1.40, respectively (cf. Table 1). To make a direct comparison to the pristine Ni_2FeGa , we evaluated the MCA and orbital moments for Ni_2FeGa without interstitials but with imposed $c/a=1.40$, resulting in an MCA of 0.066 meV and 0.170 meV per chemical formula by using Eq. (1) and Bruno’s model Eq. (2), respectively. Again, the MAEs obtained from the Bruno’s model can be well compared with that from Eq. (1) for Ni_2FeGa with C and N interstitial, but not for H interstitial case and parent compound.

The remarkable variation of the orbital moments and the resulting significant enhancement of MCAs can be attributed to the atoms surrounding the interstitial atoms. It is noted that C and N interstitials can give rise a significant MCA to Ni_2FeGa , while the effect of H interstitial is rather weaker. Following Table 2, it is clear that without interstitials ($c/a=1.40$), Fe atoms have the leading contribution to the MCA of 0.26 meV per atom, while the contribution from Ni (about -0.039 meV per atom) is an order of magnitude lower with opposite sign. The change in c/a from 1.35 to 1.40 has minor influence on the MCA and orbit moment. After considering interstitial N (H), the contribution for Ni-i atoms within the same plane is enhanced to 0.250 meV (0.097 meV) per atom. As to C interstitial atoms, the MCA of Ni-i atoms is slightly (Fig. 1(b)) increased to 0.039 meV per atom. That is, all types of the interstitial atoms lead to a sign change of the contribution to MCA for Ni-i. On the other hand, the orbital moments and thus the resulting MCA contribution are very comparable for the

Ni-ii atoms with and without interstitials, because the Ni-ii atoms are far away from the interstitials. Furthermore, for the H interstitial case, both the MCA and orbital moments of all Fe (including iii, iv and v) atoms change only slightly comparing to those in the pristine compound with imposed $c/a=1.40$, whereas the N and C interstitials lead to significant enhancement of contribution for Fe-iii atoms to MCA. For instance, the MCA contributions of Fe-iii atoms below the interstitials are increased to 0.681 meV and 0.508 meV per atom with N and C interstitials, more than two times larger than (0.260 meV) in the parent compound. Meanwhile the contributions from Fe-iv and Fe-v atoms are slightly reduced. Therefore, the interstitial atoms have very strong influence on the MCA of the local surrounding atoms, while the global tetragonal distortion has relatively marginal effects.

The effects of interstitials on MCAs and orbital magnetizations can be further understood based on the chemical bonding pairs between the interstitials and surrounding magnetic atoms. For instance, the octahedral center (interstitial) H, C and N to octahedral planar corner Ni-i almost have the same bond lengths as 1.85 Å, 1.88 Å and 1.88 Å. However, the integrated COHP of H-Ni bond is just -0.63 eV, which is much weaker than that of the comparable bond strength of C-(Ni-i) (-2.12 eV) and N-(Ni-i) (-1.96 eV) bonds. On the other hand, the octahedral below corner Fe-iii to the interstitial H, C and N have similar bond lengths as 1.65 Å, 1.83 Å and 1.83 Å, while the bond integrated COHP of H-Fe (iii) (-1.24 eV) can be comparable to that of C-(Fe-iii) (-2.88 eV) and N-(Fe-iii) (-2.38 eV) bonds. Obviously, the bond strengths of C interstitial to Fe-iii) and Ni-i are the strongest. This explains the significant change of orbital moments of Ni_2FeGa with C interstitial comparing to Ni_2FeGa at the same tetragonal distortion ratio without interstitial. In this view, the H interstitial just induce tetragonal distortion to Ni_2FeGa , while C and N interstitial not only induce tetragonal distortion but also change the chemical environment by forming strong bonds. We notice that the interstitial to planer Ni-i atom have comparable bond lengths as to lower Fe-iii atoms but weaker integrated COHP for each interstitial cases. Such bonding behaviors explains the effect of

interstitial on the magnetization and the MCA for Fe-iii atoms is stronger than that for Ni-i atoms.

4. Conclusion

Based on high-throughput DFT calculations, we investigated the effects of (H, B, C, and N) interstitials on the magnetic properties of cubic full Heusler compounds. We identified 32 compounds with substantial uniaxial MAE. Detailed analysis reveals that in addition to the breaking of the cubic symmetry, the changes in the local crystalline environment can induce significant contribution to the MAE, which can be attributed to the chemical bonding between the interstitial and surrounding magnetic atoms. This could provide an efficient way to design permanent magnets, which shall be explored further both experimentally and theoretically.

ACKNOWLEDGMENTS

Qiang Gao thanks the financial support from the China Scholarship Council. The authors gratefully acknowledge computational time on the Lichtenberg High Performance Supercomputer.

References

- [1] O. Gutfleisch, M. A. Willard, E. Brück, C. H. Chen, S. G. Sankar, J. P. Liu, Magnetic materials and devices for the 21st century: Stronger, lighter, and more energy efficient, *Advanced Materials* 23 (7) (2011) 821–842. doi:10.1002/adma.201002180. URL <https://onlinelibrary.wiley.com/doi/abs/10.1002/adma.201002180>
- [2] J. M. D. Coey, Permanent magnets: Plugging the gap, *Scripta Materialia* 67 (6) (2012) 524–529. doi:10.1016/j.scriptamat.2012.04.036. URL <http://www.sciencedirect.com/science/article/pii/S1359646212002990>
- [3] S. Sugimoto, Current status and recent topics of rare-earth permanent magnets, *Journal of Physics D: Applied Physics* 44 (6) (2011) 064001. doi:10.1088/0022-3727/44/6/064001. URL <https://doi.org/10.1088/2F0022-3727/2F44/2F6/2F064001>

- [4] K. P. Skokov, O. Gutfleisch, Heavy rare earth free, free rare earth and rare earth free magnets - vision and reality, *Scripta Materialia* 154 (2018) 289–294. doi:10.1016/j.scriptamat.2018.01.032.
URL <http://www.sciencedirect.com/science/article/pii/S1359646218300599>
- [5] T. Burkert, L. Nordström, O. Eriksson, O. Heinonen, Giant magnetic anisotropy in tetragonal fcco alloys, *Physical Review Letters* 93 (2) (2004) 027203. doi:10.1103/PhysRevLett.93.027203.
URL <https://link.aps.org/doi/10.1103/PhysRevLett.93.027203>
- [6] G. Andersson, T. Burkert, P. Warnicke, M. Björck, B. Sanyal, C. Chacon, C. Zlotea, L. Nordström, P. Nordblad, O. Eriksson, Perpendicular magnetocrystalline anisotropy in tetragonally distorted Fe-Co Alloys, *Physical Review Letters* 96 (3) (2006) 037205. doi:10.1103/PhysRevLett.96.037205.
URL <https://link.aps.org/doi/10.1103/PhysRevLett.96.037205>
- [7] F. Yildiz, M. Przybylski, X.-D. Ma, J. Kirschner, Strong perpendicular anisotropy in Fe_{1-x}Cox alloy films epitaxially grown on mismatching Pd (001), Ir (001), and Rh (001) *Physical Review B* 80 (6) (2009) 064415. doi:10.1103/PhysRevB.80.064415.
URL <https://link.aps.org/doi/10.1103/PhysRevB.80.064415>
- [8] F. Luo, X. L. Fu, A. Winkelmann, M. Przybylski, Tuning the perpendicular magnetic anisotropy in tetragonally distorted fexco_{1-x} alloy films on rh (001) by varying the alloy *Applied Physics Letters* 91 (26) (2007) 262512. doi:10.1063/1.2821370.
URL <https://aip.scitation.org/doi/abs/10.1063/1.2821370>
- [9] L. Reichel, L. Schultz, S. Fähler, Lattice relaxation studies in strained epitaxial Fe-Co-C films, *Journal of Applied Physics* 117 (17) (2015) 17C712. doi:10.1063/1.4908031.
URL <https://aip.scitation.org/doi/10.1063/1.4908031>
- [10] L. Reichel, L. Schultz, D. Pohl, S. Oswald, S. Fähler, M. Werwiński, A. Edström, E. K. Delczeg-Czirjak, J. Ruzs, From soft to hard magnetic Fe-Co-B by spontaneous strain: a combined first principles and thin film study, *Journal of Physics: Condensed Matter* 27 (47) (2015) 476002. doi:10.1088/0953-8984/27/47/476002.
URL <https://doi.org/10.1088/0953-8984/27/47/476002>
- [11] H. Zhang, I. Dirba, T. Helbig, L. Alff, O. Gutfleisch, Engineering perpendicular magnetic anisotropy in Fe via interstitial nitrogenation: N choose K, *APL Materials* 4 (11) (2016) 116104. doi:10.1063/1.4967285.
URL <https://aip.scitation.org/doi/abs/10.1063/1.4967285>

- [12] D. Gölden, H. Zhang, I. Radulov, I. Dirba, P. Komissinskiy, E. Hildebrandt, L. Alff, Evolution of anisotropy in bcc Fe distorted by interstitial boron, *Physical Review B* 97 (1) (2018) 014411. doi:10.1103/PhysRevB.97.014411.
URL <https://link.aps.org/doi/10.1103/PhysRevB.97.014411>
- [13] S. V. Faleev, Y. Ferrante, J. Jeong, M. G. Samant, B. Jones, S. S. P. Parkin, Heusler compounds with perpendicular magnetic anisotropy and large tunneling magnetoresistance, *Physical Review Materials* 1 (2) (2017) 024402. doi:10.1103/PhysRevMaterials.1.024402.
URL <https://link.aps.org/doi/10.1103/PhysRevMaterials.1.024402>
- [14] Y.-I. Matsushita, G. Madjarova, J. K. Dewhurst, S. Shallcross, C. Felser, S. Sharma, E. K. U. Gross, Large magnetocrystalline anisotropy in tetragonally distorted heuslers: a systematic study, *Journal of Physics D: Applied Physics* 50 (9) (2017) 095002. doi:10.1088/1361-6463/aa5441.
URL <https://doi.org/10.1088/1361-6463/aa5441>
- [15] H. C. Herper, Ni-based heusler compounds: How to tune the magnetocrystalline anisotropy, *Physical Review B* 98 (1) (2018) 014411. doi:10.1103/PhysRevB.98.014411.
URL <https://link.aps.org/doi/10.1103/PhysRevB.98.014411>
- [16] M. J. Pechan, C. Yu, D. Carr, C. J. Palmstrøm, Remarkable strain-induced magnetic anisotropy in epitaxial Co₂MnGa (001) films, *Journal of Magnetism and Magnetic Materials* 286 (2005) 340–345. doi:10.1016/j.jmmm.2004.09.090.
URL <http://www.sciencedirect.com/science/article/pii/S0304885304009850>
- [17] Y. Zhang, J. Liu, Q. Zheng, J. Zhang, W. Xia, J. Du, A. Yan, Large magnetic entropy change and enhanced mechanical properties of Ni-Mn-Sn-C alloys, *Scripta Materialia* 75 (2014) 26–29. doi:10.1016/j.scriptamat.2013.11.009.
URL <http://www.sciencedirect.com/science/article/pii/S1359646213005666>
- [18] I. Dubenko, T. Samanta, A. Quetz, A. Kazakov, I. Rodionov, D. Mettus, V. Prudnikov, S. Stadler, P. Adams, J. Prestigiacomo, A. Granovsky, A. Zhukov, N. Ali, The comparison of direct and indirect methods for determining the magnetocaloric parameters in the Heusler alloy Ni₅₀Mn₅₀, *Applied Physics Letters* 100 (19) (2012) 192402. doi:10.1063/1.4714539.
URL <https://aip.scitation.org/doi/abs/10.1063/1.4714539>
- [19] H. C. Xuan, D. H. Wang, C. L. Zhang, Z. D. Han, B. X. Gu, Y. W. Du, Boron's effect on martensitic transformation and magnetocaloric effect in Ni₄₃Mn₄₆Sn₁₁B_x alloys, *Applied Physics Letters* 92 (10) (2008) 102503. doi:10.1063/1.2895645.
URL <https://aip.scitation.org/doi/abs/10.1063/1.2895645>

- [20] N. V. Nong, L. T. Tai, N. T. Huy, N. T. Trung, C. R. H. Bahl, R. Venkatesh, F. W. Poulsen, N. Pryds, Structural, magnetic and magnetocaloric properties of Heusler alloys Ni₅₀Mn₃₈Sb₁₂ with boron addition, *Materials Science and Engineering: B* 176 (16) (2011) 1322–1325. doi:10.1016/j.mseb.2011.07.013. URL <http://www.sciencedirect.com/science/article/pii/S0921510711003345>
- [21] http://www2.fiz.karlsruhe.de/icsd_home.html. [link]. URL http://www2.fiz-karlsruhe.de/icsd_home.html
- [22] I. Opahle, G. K. H. Madsen, R. Drautz, High throughput density functional investigations of the stability, electronic structure, Physical Chemistry Chemical Physics 14 (47) (2012) 16197–16202. doi:10.1039/C2CP41826F. URL <https://pubs.rsc.org/en/content/articlelanding/2012/cp/c2cp41826f>
- [23] I. Opahle, A. Parma, E. J. McEniry, R. Drautz, G. K. H. Madsen, High-throughput study of the structural stability and thermoelectric properties of transition metal silicides, *New Journal of Physics* 15 (10) (2013) 105010. doi:10.1088/1367-2630/15/10/105010. URL <https://doi.org/10.1088%2F1367-2630%2F15%2F10%2F105010>
- [24] G. Kresse, J. Furthmüller, Efficient iterative schemes for ab initio total-energy calculations using a plane-wave basis set, *Physical Review B* 54 (16) (1996) 11169–11186. doi:10.1103/PhysRevB.54.11169. URL <https://link.aps.org/doi/10.1103/PhysRevB.54.11169>
- [25] G. Kresse, D. Joubert, From ultrasoft pseudopotentials to the projector augmented-wave method, *Physical Review B* 59 (3) (1999) 1758–1775. doi:10.1103/PhysRevB.59.1758. URL <https://link.aps.org/doi/10.1103/PhysRevB.59.1758>
- [26] K. Koepernik, H. Eschrig, Full-potential nonorthogonal local-orbital minimum-basis band-structure scheme, *Physical Review B* 59 (3) (1999) 1743–1757. doi:10.1103/PhysRevB.59.1743. URL <https://link.aps.org/doi/10.1103/PhysRevB.59.1743>
- [27] I. Opahle, K. Koepernik, H. Eschrig, Full-potential band-structure calculation of iron pyrite, *Physical Review B* 60 (20) (1999) 14035–14041. doi:10.1103/PhysRevB.60.14035. URL <https://link.aps.org/doi/10.1103/PhysRevB.60.14035>
- [28] D. Vanderbilt, Soft self-consistent pseudopotentials in a generalized eigenvalue formalism, *Physical Review B* 41 (11) (1990) 7892–7895. doi:10.1103/PhysRevB.41.7892. URL <https://link.aps.org/doi/10.1103/PhysRevB.41.7892>
- [29] J. P. Perdew, J. A. Chevary, S. H. Vosko, K. A. Jackson, M. R. Pederson, D. J. Singh, C. Fiolhais, Atoms, molecules, solids, and surfaces: Applications of the generalized gradient approximation for exchange and correlation,

- Physical Review B 46 (11) (1992) 6671–6687. doi:10.1103/PhysRevB.46.6671.
 URL <https://link.aps.org/doi/10.1103/PhysRevB.46.6671>
- [30] J. P. Perdew, K. Burke, M. Ernzerhof, Generalized Gradient Approximation Made Simple, Physical Review Letters 77 (18) (1996) 3865–3868. doi:10.1103/PhysRevLett.77.3865.
 URL <https://link.aps.org/doi/10.1103/PhysRevLett.77.3865>
- [31] V. L. Deringer, A. L. Tchougréeff, R. Dronskowski, Crystal Orbital Hamilton Population (COHP) Analysis As Projected from Plane-Wave Basis Sets, The Journal of Physical Chemistry A 115 (21) (2011) 5461–5466. doi:10.1021/jp202489s.
 URL <https://doi.org/10.1021/jp202489s>
- [32] H. Masumoto, K. Watanabe, New Compounds of the Clb, Cl Types of RhMnSb, IrMnSn and IrMnAl, New L21 (Heusler) Type, Journal of the Physical Society of Japan 32 (1) (1972) 281–281. doi:10.1143/JPSJ.32.281.
 URL https://www.jstage.jst.go.jp/article/jpsj1946/32/1/32_1_281/_article/-char/ja/
- [33] J. Balluff, K. Diekmann, G. Reiss, M. Meinert, High-throughput screening for antiferromagnetic Heusler compounds using density functional theory, Physical Review Materials 1 (3) (2017) 034404. doi:10.1103/PhysRevMaterials.1.034404.
 URL <https://link.aps.org/doi/10.1103/PhysRevMaterials.1.034404>
- [34] K. Ramesh Kumar, N. Harish Kumar, G. Markandeyulu, J. Arout Chelvane, V. Neu, P. D. Babu, Structural, magnetic and transport properties of half-metallic ferrimagnet Mn₂vga, Journal of Magnetism and Magnetic Materials 320 (21) (2008) 2737–2740. doi:10.1016/j.jmmm.2008.06.003.
 URL <http://www.sciencedirect.com/science/article/pii/S0304885308006926>
- [35] J. C. Suits, Structural instability in new magnetic heusler compounds, Solid State Communications 18 (3) (1976) 423–425. doi:10.1016/0038-1098(76)90040-5.
 URL <http://www.sciencedirect.com/science/article/pii/0038109876900405>
- [36] A. Sakuma, First Principle Calculation of the Magnetocrystalline Anisotropy Energy of FePt and CoPt Ordered Alloys, Journal of the Physical Society of Japan 63 (8) (1994) 3053–3058. doi:10.1143/jpsj.63.3053.
 URL https://www.jstage.jst.go.jp/article/jpsj/63/8/63_8_3053/_article/-char/ja/
- [37] Y. Kota, A. Sakuma, Relationship between Magnetocrystalline Anisotropy and Orbital Magnetic Moment in L10-Type Ordered Alloys, Journal of the Physical Society of Japan 81 (8) (2012) 084705. doi:10.1143/JPSJ.81.084705.
 URL <https://journals.jps.jp/doi/10.1143/JPSJ.81.084705>

- [38] Y. Yamada, T. Suzuki, H. Kanazawa, J. C. Österman, The origin of the large perpendicular magnetic anisotropy in Co₃Pt alloy thin films, *Journal of Applied Physics* 85 (8) (1999) 5094–5096. doi:10.1063/1.370101. URL <https://aip.scitation.org/doi/abs/10.1063/1.370101>
- [39] H. R. Kirchmayr, Permanent magnets and hard magnetic materials, *Journal of Physics D: Applied Physics* 29 (11) (1996) 2763–2778. doi:10.1088/0022-3727/29/11/007. URL <https://doi.org/10.1088/0022-3727/29/11/007>
- [40] J. Cui, M. Kramer, L. Zhou, F. Liu, A. Gabay, G. Hadjipanayis, B. Balasubramanian, D. Sellmyer, Current progress and future challenges in rare-earth-free permanent magnets, *Acta Materialia* 158 (2018) 118–137. doi:10.1016/j.actamat.2018.07.049. URL <http://www.sciencedirect.com/science/article/pii/S1359645418305858>
- [41] N. K. Jaggi, K. R. P. M. Rao, A. K. Grover, L. C. Gupta, R. Vijayaraghavan, D. Le Khoi, Mossbauer and NMR study of site preference and local environment effects in Co₂FeGa & Fe₂CoGa, *Hyperfine Interactions* 4 (1) (1978) 402–406. doi:10.1007/BF01021860. URL <https://doi.org/10.1007/BF01021860>
- [42] T. Gasi, V. Ksenofontov, J. Kiss, S. Chadov, A. K. Nayak, M. Nicklas, J. Winterlik, M. Schwall, P. Klaer, P. Adler, C. Felser, Iron-based Heusler compounds Fe₂YZ: Comparison with theoretical predictions of the crystal structure and magnetism, *Physical Review B* 87 (6) (2013) 064411. doi:10.1103/PhysRevB.87.064411. URL <https://link.aps.org/doi/10.1103/PhysRevB.87.064411>
- [43] A. Dannenberg, M. Siewert, M. E. Gruner, M. Wuttig, P. Entel, Competing structural ordering tendencies in Heusler-type alloys with high Curie temperatures: Fe₂CoGa_{1-x}Zn_x studied by neutron diffraction, *Physical Review B* 82 (21) (2010) 214421. doi:10.1103/PhysRevB.82.214421. URL <https://link.aps.org/doi/10.1103/PhysRevB.82.214421>
- [44] Z. H. Liu, M. Zhang, Y. T. Cui, Y. Q. Zhou, W. H. Wang, G. H. Wu, X. X. Zhang, G. Xiao, Martensitic transformation and shape memory effect in ferromagnetic Heusler alloy Ni₂FeGa, *Applied Physics Letters* 82 (3) (2003) 424–426. doi:10.1063/1.1534612. URL <https://aip.scitation.org/doi/abs/10.1063/1.1534612>
- [45] J. F. Qian, H. G. Zhang, J. L. Chen, W. H. Wang, G. H. Wu, Undercooling growth and magnetic characterization of ferromagnetic shape memory alloy Ni₂FeGa single crystals, *Journal of Crystal Growth* 388 (2014) 107–111. doi:10.1016/j.jcrysgro.2013.11.016. URL <http://www.sciencedirect.com/science/article/pii/S0022024813007689>

- [46] V. Recarte, J. I. Pérez-Landazábal, C. Gómez-Polo, E. Cesari, J. Dutkiewicz, Magnetocaloric effect in Ni-Fe-Ga shape memory alloys, *Applied Physics Letters* 88 (13) (2006) 132503. doi:10.1063/1.2189665.
URL <https://aip.scitation.org/doi/10.1063/1.2189665>
- [47] Y. Qawasmeh, B. Hamad, Investigation of the structural, electronic, and magnetic properties of Ni-based Heusler alloys from *Journal of Applied Physics* 111 (3) (2012) 033905. doi:10.1063/1.3681286.
URL <https://aip.scitation.org/doi/10.1063/1.3681286>
- [48] S. R. Barman, A. Chakrabarti, S. Singh, S. Banik, S. Bhardwaj, P. L. Paulose, B. A. Chalke, A. K. Panda, A. Mitra, A. M. Awasthi, Theoretical prediction and experimental study of a ferromagnetic shape memory alloy: Ga_2MnNi , *Physical Review B* 78 (13) (2008) 134406. doi:10.1103/PhysRevB.78.134406.
URL <https://link.aps.org/doi/10.1103/PhysRevB.78.134406>
- [49] P. Bruno, Tight-binding approach to the orbital magnetic moment and magnetocrystalline anisotropy of transition-metal monoxides, *Physical Review B* 39 (1) (1989) 865–868. doi:10.1103/PhysRevB.39.865.
URL <https://link.aps.org/doi/10.1103/PhysRevB.39.865>
- [50] Y. Liu, Z. Xu, P. D. Johnson, G. van der Laan, Spin-orbit coupling, exchange interaction, and hybridization in the photoexcitation of the Ni 3p core level, *Physical Review B* 52 (12) (1995) R8593–R8596. doi:10.1103/PhysRevB.52.R8593.
URL <https://link.aps.org/doi/10.1103/PhysRevB.52.R8593>
- [51] D. Dai, H. Xiang, M.-H. Whangbo, Effects of spin-orbit coupling on magnetic properties of discrete and extended magnetic systems, *Journal of Computational Chemistry* 29 (13) (2008) 2187–2209. doi:10.1002/jcc.21011.
URL <https://www.onlinelibrary.wiley.com/doi/abs/10.1002/jcc.21011>

Captions

Figure captions:

Figure 1: (a) The possible interstitial sites in the convention Austenite unit cell of full Heusler compounds X_2YZ . The blue and green octahedrons denote the 24f (0.25,0,0) and 24g (0.5,0.25,0.25) interstitial sites, while the red and pink tetrahedrons mark the 16e(0.125,0.875,0.875) and 16e(0.875,0.625,0.875) interstitial sites. (b) The crystal structure for the tetragonal full Heusler compound Ni_2FeGa with interstitial (int.) at the most stable octahedral sites.

Figure 2: Total energy as a function of tetragonal distortion ratio (c/a) for Fe_2CoGa with and without interstitials. The reference energy is the energy of the compound in cubic inverse Heusler structure for Fe_2CoGa with each interstitial as well as the parent compound. The opened and filled symbols represent the results Fe_2CoGa in inverse and full Heusler structures, respectively. (b) The total energy as a function of tetragonal distortion ratio for Ni_2FeGa in full Heusler structure with and without interstitials. Here the reference energy is the energy of the compound in cubic full Heusler structure.

Table captions:

Table 1: The basic information of the most promising candidates of Heusler compounds with interstitials, where “site” marks the energetically preferred interstitial site, ΔH indicate the formation energy in unit of eV/atom, c/a ratio of resulting lattice constants along c -axis and in-plane, MAE in MJ/m^3 and $meV/f.u.$ (in parenthesis), total magnetic moment M_{tot} in the unit of $\mu_B/f.u.$, and the magnetization M/V in the unit of $\mu_B/\text{\AA}^3$. It should be notices the general chemical formula for Heusler compound with interstitial is $X_2YZI_{1/4}$, where I is the interstitial.

Table 2: The orbital moment (μ_l , in unit of μ_B) and the magneto-crystalline anisotropy energy (MCA, in unit of meV) energy values for Ni_2FeGa with and without interstitials. Here the MCA is evaluated from Bruno’s formula. μ_l and \sum (in unit of meV) denote the difference of orbital moment between two magnetization directions ([001] and [100]) and the summation of MCA energy, respectively. The general chemical formula for Heusler Ni_2FeGa with interstitial is $Ni_2FeGaI_{1/4}$, where I is the interstitial.

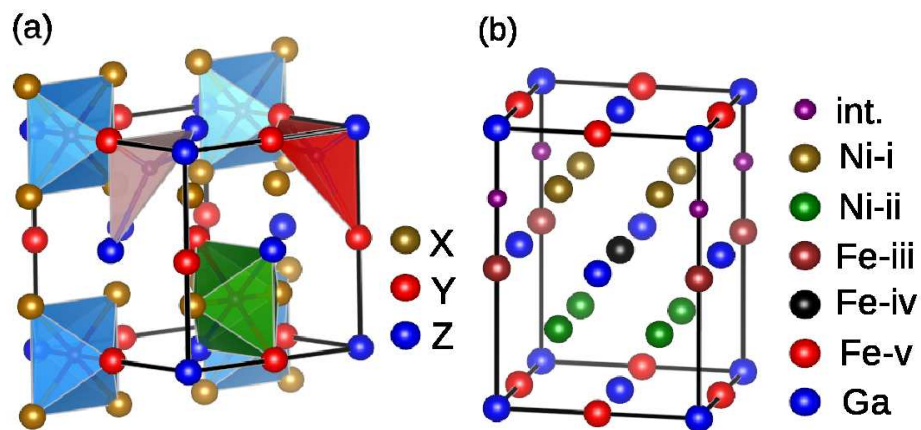


Figure 1:

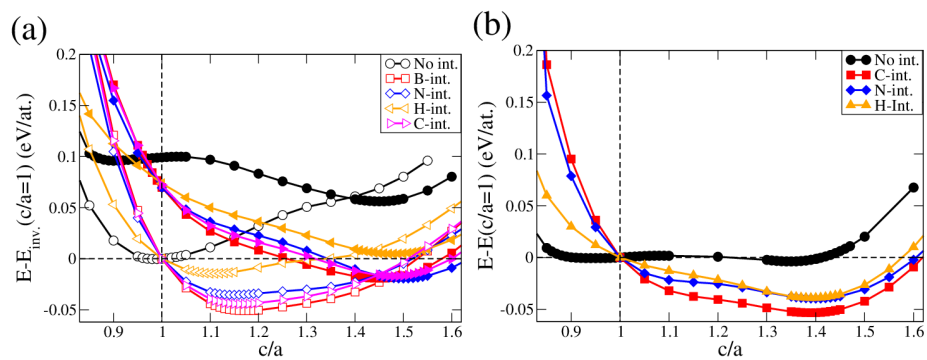


Figure 2:

Figures

Tables

Table 1:

Parent	int.	site	ΔH	c/a	MAE	M_{tot}	M/V
Fe ₂ CoGa	B	24f	-0.0616	1.45	1.4949 (0.4998)	5.56	0.1120
	C	24f	-0.0486	1.48	1.3017 (0.4072)	5.37	0.1092
	N	24f	-0.1088	1.50	1.3180 (0.4295)	5.36	0.1089
	H	24f	-0.0922	1.48	2.3677 (0.6863)	5.95	0.1227
Ni ₂ FeGa	C	24f	-0.1207	1.40	0.9636 (0.2961)	2.93	0.0595
	N	24f	-0.1620	1.40	1.4292 (0.4386)	2.97	0.0602
	H	24f	-0.1916	1.39	0.5582 (0.1668)	3.13	0.0654
Fe ₂ CoGe	H	24f	-0.0627	1.51	0.6291 (0.2080)	5.48	0.1142
	N	24f	-0.0576	1.56	0.4047 (0.1368)	5.01	0.1025
Fe ₂ NiAl	H	24f	-0.2545	1.53	0.4947 (0.1298)	4.56	0.0955
	N	24f	-0.2842	1.57	0.5270 (0.1368)	4.40	0.0902
Fe ₂ NiGa	H	24f	-0.1915	1.55	0.5670 (0.1298)	4.67	0.0977
	B	24f	-0.1219	1.51	0.7853 (0.1758)	4.42	0.0893
	C	24f	-0.1208	1.53	0.9217 (0.1863)	4.31	0.0874
	N	24f	-0.1620	1.53	1.3295 (0.2429)	4.45	0.0939
Co ₂ MnGa	C	24f	-0.1289	1.13	0.5267 (0.6303)	4.52	0.0920
	N	24f	-0.1836	1.12	0.4755 (0.1576)	4.76	0.0922
Co ₂ MnGe	C	24f	-0.0788	1.25	0.5388 (0.1226)	4.06	0.0831
	N	24f	-0.1226	1.29	0.5476 (0.1325)	4.13	0.0841
Co ₂ MnSi	C	24f	-0.2571	1.21	0.5384 (0.1464)	4.16	0.0898
Rh ₂ MnAl	C	24f	-0.5088	1.10	0.9501 (0.3336)	4.25	0.0742
	N	24f	-0.5457	1.06	1.1675 (0.4487)	4.49	0.0784
Rh ₂ NiSn	H	24f	-0.2288	1.26	0.8236 (0.3063)	0.99	0.0166
Mn ₂ VGa	C	24f	-0.1533	1.20	1.5038 (0.4874)	2.26	0.0435
	B	24f	-0.1474	1.23	1.8263 (0.5987)	2.48	0.0472
	N	24f	-0.2377	1.21	1.2674 (0.4087)	2.34	0.0451
Co ₂ FeAl	N	24g	-0.2770	1.08	0.4881 (0.3009)	5.01	0.1038
Au ₂ MnAl	H	16e	-0.1835	0.92	0.7732 (0.6489)	3.82	0.0582
	N	24g	-0.1975	1.27	-0.4091 (-0.2412)	3.66	0.0476
	C	24g	-0.2770	1.21	-0.5271 (-0.4923)	3.82	0.0574
Ni ₂ MnIn	C	24f	-0.0057	1.21	-1.0288 (-0.3513)	3.96	0.0685
Ni ₂ MnGa	H	24f	-0.2519	1.27	-1.3278 (-0.4898)	4.20	0.0852
	B	24f	-0.2204	1.28	-0.5822 (-0.1850)	4.02	0.0788
	C	24f	-0.1780	1.29	-0.9573 (-0.3031)	3.91	0.0771
Fe ₃ Ge	H	24f	-0.0563	1.42	1.5018 (0.4655)	6.44	0.1319
	B	24f	-0.0254	1.16	0.5868 (0.1812)	5.54	0.1211
Fe ₃ Ga	B	24f	-0.0710	1.21	0.6896 (0.2142)	6.16	0.1229
	N	24f	-0.1101	1.19	0.5184 (0.1610)	5.92	0.1022
Ni ₂ MnSn	B	24g	-0.0959	1.06	-0.6747 (-0.2064)	3.75	0.0645
	C	24g	-0.0480	1.17	-0.4261 (-0.1421)	3.70	0.0653
	N	24g	-0.0892	1.17	-0.4756 (-0.1613)	3.74	0.0697
Rh ₂ MnSn	C	24f	-0.2679	1.26	-0.8846 (-0.3529)	3.66	0.0572

Table 2:

	int.		Ni-i	Ni-ii	Fe-iii	Fe-iv	Fe-v	Σ
with int.	H	[001]	0.024	0.020	0.068	0.063	0.066	-
		[100]	0.019	0.022	0.043	0.040	0.046	-
		Δ	0.005	-0.002	0.025	0.023	0.020	-
		MCA	0.097	-0.039	0.309	0.284	0.247	0.330
	N	[001]	0.025	0.020	0.068	0.067	0.072	-
		[100]	0.012	0.024	0.013	0.053	0.049	-
		Δ	0.013	-0.004	0.055	0.014	0.023	-
		MCA	0.250	-0.078	0.681	0.173	0.285	0.528
	C	[001]	0.013	0.022	0.058	0.067	0.073	-
		[100]	0.011	0.024	0.017	0.048	0.051	-
		Δ	0.002	-0.002	0.041	0.019	0.021	-
		MCA	0.039	-0.039	0.508	0.235	0.260	0.316
	c/a		Ni		Fe		Σ	
w/o int.	1.35	[001]	0.022		0.065		-	
		[100]	0.024		0.044		-	
		Δ	-0.002		0.021		-	
		MCA	-0.039		0.260		0.180	
	1.40	[001]	0.021		0.061		-	
		[100]	0.023		0.041		-	
		Δ	-0.002		0.020		-	
		MCA	-0.039		0.248		0.170	

Highlights

- Rare earth free permanent magnets can be realized in tetragonally distorted full Heusler alloys induced by light interstitial atoms.
- Bain path calculations reveal that interstitials cause stable tetragonal distortion to full Heusler alloys.
- Analysis based on the perturbation theory and chemical bonding suggests that the uniaxial anisotropy can be attributed to change in the local crystalline environments around the interstitials.
- We postulate that this provides a universal way to tailor the magnetic properties of prospective permanent magnets.

A. Appendix

Table A.1: All the considered Heusler compounds (Com.) together with the ICSD ID number.

Com.	ID	Com.	ID	Com.	ID	Com.	ID
Au ₂ MnAl	57504	Co ₂ CrAl	57600	Co ₂ FeAl	57607	Co ₂ HfAl	110809
Co ₂ MnAl	606611	Co ₂ NbAl	57620	Co ₂ TaAl	606667	Co ₂ TiAl	606680
Co ₂ VAl	57643	Co ₂ ZrAl	57648	Co ₂ CrGa	102318	Co ₂ CrIn	416260
Co ₂ FeGa	102392	Co ₂ FeGe	247268	Co ₂ FeIn	102392	Co ₂ FeSi	622985
Co ₂ HfGa	102433	Co ₂ MnGa	623116	Co ₂ NbGa	623126	Co ₂ TaGa	102451
Co ₂ TiGa	102453	Co ₂ VGa	623228	Co ₂ LiGe	53673	Co ₂ MnGe	52971
Co ₂ TiGe	169469	Co ₂ ZnGe	52994	Co ₂ HfSn	102483	Co ₂ MnSb	53002
Co ₂ MnSi	106484	Co ₂ MnSn	102332	Co ₂ NbSn	102554	Co ₂ ScSn	102646
Co ₂ TiSi	53080	Co ₂ VSi	53086	Co ₂ TiSn	102583	Co ₂ VSn	102684
Co ₂ ZrSn	102687	Cu ₂ CrAl	57653	Cu ₂ MnAl	607012	Cu ₂ CoSn	103057
Cu ₂ FeSn	151205	Cu ₂ MnIn	102996	Cu ₂ MnSb	53312	Cu ₂ MnSn	103057
Cu ₂ NiSn	103069	Fe ₂ CrAl	184446	Fe ₂ MnAl	57806	Fe ₂ MoAl	57807
Fe ₂ NiAl	57808	Fe ₂ TiAl	57827	Fe ₂ VAl	57832	Fe ₂ CoGa	103473
Fe ₂ CoGe	52954	Fe ₂ CrGa	102755	Fe ₂ NiGa	103460	Fe ₂ TiGa	103469
Fe ₂ VGa	103473	Fe ₂ MnSi	632569	Fe ₂ VSi	53555	Fe ₂ TiSn	103641
Fe ₂ VSn	103644	Mn ₂ VAl	57994	Mn ₂ RhGa	247951	Mn ₂ VGa	103813
Mn ₂ RuGe	247950	Mn ₂ RuSn	247949	Mn ₂ WSn	104980	Ni ₂ CrAl	57662
Ni ₂ HfAl	57901	Ni ₂ MnAl	57976	Ni ₂ NbAl	58016	Ni ₂ ScAl	58050
Ni ₂ TaAl	58055	Ni ₂ TiAl	58063	Ni ₂ VAl	58071	Ni ₂ ZrAl	58081
Ni ₂ CuSb	53320	Ni ₂ CuSn	103068	Ni ₂ HfGa	103734	Ni ₂ MnGa	103803
Ni ₂ NbGa	103839	Ni ₂ ScGa	103874	Ni ₂ TaGa	103881	Ni ₂ TiGa	103886
Ni ₂ VGa	103892	Ni ₂ ZrGa	103902	Ni ₂ LiGe	53673	Ni ₂ MnGe	192566
Ni ₂ ZnGe	53865	Ni ₂ HfIn	54595	Ni ₂ HfSn	104250	Ni ₂ MgIn	51982
Ni ₂ MnIn	639954	Ni ₂ ScIn	59446	Ni ₂ TiIn	59451	Ni ₂ ZrIn	59460
Ni ₂ LiSi	44819	Ni ₂ LiSn	25325	Ni ₂ MgSb	104841	Ni ₂ MgSn	104842
Ni ₂ TiSb	76700	Ni ₂ ZrSb	76703	Ni ₂ ScSn	105339	Ni ₂ TiSn	105369
Ni ₂ VSn	105376	Ni ₂ ZrSn	105383	Pd ₂ MnAl	57981	Pd ₂ MnAs	107955
Ni ₂ NbSn	105181	Pd ₂ MnGe	53705	Rh ₂ NiSn	105327	Pd ₂ MnIn	51990
Pd ₂ MnSb	643312	Pd ₂ MnSn	104945	Rh ₂ MnAl	57986	Rh ₂ MnGe	53706
Rh ₂ MnPb	104936	Rh ₂ MnSn	104964	Ru ₂ FeSi	53525	Ru ₂ FeSn	103615
Fe ₃ Al	57793	Fe ₃ Ga	108436	Fe ₃ Ge	53462	Fe ₃ Si	53545
Mn ₃ Si	76227	Ni ₃ Al	58038	Ni ₃ Sb	76693	Ni ₃ Sn	105354